

Measurement of the total and leptonic decay widths of the J/ψ resonance with an energy scan method at BESIII

M. Ablikim¹, M. N. Achasov^{11,b}, P. Adlarson⁷⁰, M. Albrecht⁴, R. Aliberti³¹, A. Amoroso^{69A,69C}, M. R. An³⁵, Q. An^{66,53}, X. H. Bai⁶¹, Y. Bai⁵², O. Bakina³², R. Baldini Ferroli^{26A}, I. Balossino^{27A}, Y. Ban^{42,g}, V. Batozskaya^{1,40}, D. Becker³¹, K. Begzsuren²⁹, N. Berger³¹, M. Bertani^{26A}, D. Bettoni^{27A}, F. Bianchi^{69A,69C}, J. Bloms⁶³, A. Bortone^{69A,69C}, I. Boyko³², R. A. Briere⁵, A. Brueggemann⁶³, H. Cai⁷¹, X. Cai^{1,53}, A. Calcaterra^{26A}, G. F. Cao^{1,58}, N. Cao^{1,58}, S. A. Cetin^{57A}, J. F. Chang^{1,53}, W. L. Chang^{1,58}, G. Chelkov^{32,a}, C. Chen³⁹, Chao Chen⁵⁰, G. Chen¹, H. S. Chen^{1,58}, M. L. Chen^{1,53}, S. J. Chen³⁸, S. M. Chen⁵⁶, T. Chen¹, X. R. Chen^{28,58}, X. T. Chen¹, Y. B. Chen^{1,53}, Z. J. Chen^{23,h}, W. S. Cheng^{69C}, S. K. Choi⁵⁰, X. Chu³⁹, G. Cibinetto^{27A}, F. Cossio^{69C}, J. J. Cui⁴⁵, H. L. Dai^{1,53}, J. P. Dai⁷³, A. Dbeyssi¹⁷, R. E. de Boer⁴, D. Dedovich³², Z. Y. Deng¹, A. Denig³¹, I. Denysenko³², M. Destefanis^{69A,69C}, F. De Mori^{69A,69C}, Y. Ding³⁶, J. Dong^{1,53}, L. Y. Dong^{1,58}, M. Y. Dong^{1,53,58}, X. Dong⁷¹, S. X. Du⁷⁵, P. Egorov^{32,a}, Y. L. Fan⁷¹, J. Fang^{1,53}, S. S. Fang^{1,58}, W. X. Fang¹, Y. Fang¹, R. Farinelli^{27A}, L. Fava^{69B,69C}, F. Feldbauer⁴, G. Felici^{26A}, C. Q. Feng^{66,53}, J. H. Feng⁵⁴, K. Fischer⁶⁴, M. Fritsch⁴, C. Fritsch⁶³, C. D. Fu¹, H. Gao⁵⁸, Y. N. Gao^{42,g}, Yang Gao^{66,53}, S. Garbolino^{69C}, I. Garzia^{27A,27B}, P. T. Ge⁷¹, Z. W. Ge³⁸, C. Geng⁵⁴, E. M. Gersabeck⁶², A. Gilman⁶⁴, K. Goetzen¹², L. Gong³⁶, W. X. Gong^{1,53}, W. Gradl³¹, M. Greco^{69A,69C}, L. M. Gu³⁸, M. H. Gu^{1,53}, Y. T. Gu¹⁴, C. Y. Guan^{1,58}, A. Q. Guo^{28,58}, L. B. Guo³⁷, R. P. Guo⁴⁴, Y. P. Guo^{10,f}, A. Guskov^{32,a}, T. T. Han⁴⁵, W. Y. Han³⁵, X. Q. Hao¹⁸, F. A. Harris⁶⁰, K. K. He⁵⁰, K. L. He^{1,58}, F. H. Heinsius⁴, C. H. Heinz³¹, Y. K. Heng^{1,53,58}, C. Herold⁵⁵, M. Himmelreich^{31,d}, G. Y. Hou^{1,58}, Y. R. Hou⁵⁸, Z. L. Hou¹, H. M. Hu^{1,58}, J. F. Hu^{51,i}, T. Hu^{1,53,58}, Y. Hu¹, G. S. Huang^{66,53}, K. X. Huang⁵⁴, L. Q. Huang^{28,58}, X. T. Huang⁴⁵, Y. P. Huang¹, Z. Huang^{42,g}, T. Hussain⁶⁸, N. Hüsken^{25,31}, W. Imoehl²⁵, M. Irshad^{66,53}, J. Jackson²⁵, S. Jaeger⁴, S. Janchiv²⁹, E. Jang⁵⁰, J. H. Jeong⁵⁰, Q. Ji¹, Q. P. Ji¹⁸, X. B. Ji^{1,58}, X. L. Ji^{1,53}, Y. Y. Ji⁴⁵, Z. K. Jia^{66,53}, H. B. Jiang⁴⁵, S. S. Jiang³⁵, X. S. Jiang^{1,53,58}, Y. Jiang⁵⁸, J. B. Jiao⁴⁵, Z. Jiao²¹, S. Jin³⁸, Y. Jin⁶¹, M. Q. Jing^{1,58}, T. Johansson⁷⁰, N. Kalantar-Nayestanaki⁵⁹, X. S. Kang³⁶, R. Kappert⁵⁹, B. C. Ke⁷⁵, I. K. Keshk⁴, A. Khoukaz⁶³, R. Kiuchi¹, R. Kliemt¹², L. Koch³³, O. B. Kolcu^{57A}, B. Kopf⁴, M. Kuemmel⁴, M. Kuessner⁴, A. Kupsc^{40,70}, W. Kühn³³, J. J. Lane⁶², J. S. Lange³³, P. Larin¹⁷, A. Lavania²⁴, L. Lavezzi^{69A,69C}, Z. H. Lei^{66,53}, H. Leithoff³¹, M. Lellmann³¹, T. Lenz³¹, C. C. Li⁴³, C. C. Li³⁹, C. H. Li³⁵, Cheng Li^{66,53}, D. M. Li⁷⁵, F. Li^{1,53}, G. Li¹, H. Li⁴⁷, H. Li^{66,53}, H. B. Li^{1,58}, H. J. Li¹⁸, H. N. Li^{51,i}, J. Q. Li⁴, J. S. Li⁵⁴, J. W. Li⁴⁵, Ke Li¹, L. J. Li¹, L. K. Li¹, Lei Li³, M. H. Li³⁹, P. R. Li^{34,j,k}, S. X. Li¹⁰, S. Y. Li⁵⁶, T. Li⁴⁵, W. D. Li^{1,58}, W. G. Li¹, X. H. Li^{66,53}, X. L. Li⁴⁵, Xiaoyu Li^{1,58}, Z. X. Li¹⁴, H. Liang^{66,53}, H. Liang^{1,58}, H. Liang³⁰, Y. F. Liang⁴⁹, Y. T. Liang^{28,58}, G. R. Liao¹³, L. Z. Liao⁴⁵, J. Libby²⁴, A. Limphirat⁵⁵, C. X. Lin⁵⁴, D. X. Lin^{28,58}, T. Lin¹, B. J. Liu¹, C. X. Liu¹, D. Liu^{17,66}, F. H. Liu⁴⁸, Fang Liu¹, Feng Liu⁶, G. M. Liu^{51,i}, H. Liu^{34,j,k}, H. B. Liu¹⁴, H. M. Liu^{1,58}, Huanhuan Liu¹, Huihui Liu¹⁹, J. B. Liu^{66,53}, J. L. Liu⁶⁷, J. Y. Liu^{1,58}, K. Liu¹, K. Y. Liu³⁶, Ke Liu²⁰, L. Liu^{66,53}, Lu Liu³⁹, M. H. Liu^{10,f}, P. L. Liu¹, Q. Liu⁵⁸, S. B. Liu^{66,53}, T. Liu^{10,f}, W. K. Liu³⁹, W. M. Liu^{66,53}, X. Liu^{34,j,k}, Y. Liu^{34,j,k}, Y. B. Liu³⁹, Z. A. Liu^{1,53,58}, Z. Q. Liu⁴⁵, X. C. Lou^{1,53,58}, F. X. Lu⁵⁴, H. J. Lu²¹, J. G. Lu^{1,53}, X. L. Lu¹, Y. Lu⁷, Y. P. Lu^{1,53}, Z. H. Lu¹, C. L. Luo³⁷, M. X. Luo⁷⁴, T. Luo^{10,f}, X. L. Luo^{1,53}, X. R. Lyu⁵⁸, Y. F. Lyu³⁹, F. C. Ma³⁶, H. L. Ma¹, L. L. Ma⁴⁵, M. M. Ma^{1,58}, Q. M. Ma¹, R. Q. Ma^{1,58}, R. T. Ma⁵⁸, X. Y. Ma^{1,53}, Y. Ma^{42,g}, F. E. Maas¹⁷, M. Maggiora^{69A,69C}, S. Maldaner⁴, S. Malde⁶⁴, Q. A. Malik⁶⁸, A. Mangoni^{26B}, Y. J. Mao^{42,g}, Z. P. Mao¹, S. Marcello^{69A,69C}, Z. X. Meng⁶¹, G. Mezzadri^{27A}, H. Miao¹, T. J. Min³⁸, R. E. Mitchell²⁵, X. H. Mo^{1,53,58}, N. Yu. Muchnoi^{11,b}, Y. Nefedov³², F. Nerling^{17,d}, I. B. Nikolaev^{11,b}, Z. Ning^{1,53}, S. Nisar^{9,l}, Y. Niu⁴⁵, S. L. Olsen⁵⁸, Q. Ouyang^{1,53,58}, S. Pacetti^{26B,26C}, X. Pan^{10,f}, Y. Pan⁵², A. Pathak³⁰, M. Pelizaeus⁴, H. P. Peng^{66,53}, K. Peters^{12,d}, J. L. Ping³⁷, R. G. Ping^{1,58}, S. Plura³¹, S. Pogodin³², V. Prasad^{66,53}, F. Z. Qi¹, H. Qi^{66,53}, H. R. Qi⁵⁶, M. Qi³⁸, T. Y. Qi^{10,f}, S. Qian^{1,53}, W. B. Qian⁵⁸, Z. Qian⁵⁴, C. F. Qiao⁵⁸, J. J. Qin⁶⁷, L. Q. Qin¹³, X. P. Qin^{10,f}, X. S. Qin⁴⁵, Z. H. Qin^{1,53}, J. F. Qiu¹, S. Q. Qu³⁹, S. Q. Qu⁵⁶, K. H. Rashid⁶⁸, C. F. Redmer³¹, K. J. Ren³⁵, A. Rivetti^{69C}, V. Rodin⁵⁹, M. Rolo^{69C}, G. Rong^{1,58}, Ch. Rosner¹⁷, S. N. Ruan³⁹, H. S. Sang⁶⁶, A. Sarantsev^{32,c}, Y. Schelhaas³¹, C. Schnier⁴, K. Schoenning⁷⁰, M. Scodeggio^{27A,27B}, K. Y. Shan^{10,f}, W. Shan²², X. Y. Shan^{66,53}, J. F. Shanguan⁵⁰, L. G. Shao^{1,58}, M. Shao^{66,53}, C. P. Shen^{10,f}, H. F. Shen^{1,58}, X. Y. Shen^{1,58}, B. A. Shi⁵⁸, H. C. Shi^{66,53}, J. Y. Shi¹, q. q. Shi⁵⁰, R. S. Shi^{1,58}, X. Shi^{1,53}, X. D. Shi^{66,53}, J. J. Song¹⁸, W. M. Song^{30,1}, Y. X. Song^{42,g}, S. Sosio^{69A,69C}, S. Spataro^{69A,69C}, F. Stierli³¹, K. X. Su⁷¹, P. P. Su⁵⁰, Y. J. Su⁵⁸, G. X. Sun¹, H. Sun⁵⁸, H. K. Sun¹, J. F. Sun¹⁸, L. Sun⁷¹, S. S. Sun^{1,58}, T. Sun^{1,58}, W. Y. Sun³⁰, X. Sun^{23,h}, Y. J. Sun^{66,53}, Y. Z. Sun¹, Z. T. Sun⁴⁵, Y. H. Tan⁷¹, Y. X. Tan^{66,53}, C. J. Tang⁴⁹, G. Y. Tang¹, J. Tang⁵⁴, L. Y. Tao⁶⁷, Q. T. Tao^{23,h}, M. Tat⁶⁴, J. X. Teng^{66,53}, V. Thoren⁷⁰, W. H. Tian⁴⁷, Y. Tian^{28,58}, I. Uman^{57B}, B. Wang¹, B. L. Wang⁵⁸, C. W. Wang³⁸, D. Y. Wang^{42,g}, F. Wang⁶⁷, H. J. Wang^{34,j,k}, H. P. Wang^{1,58}, K. Wang^{1,53}, L. L. Wang¹, M. Wang⁴⁵, M. Z. Wang^{42,g}, Meng Wang^{1,58}, S. Wang¹³, S. Wang^{10,f}, T. Wang^{10,f}, T. J. Wang³⁹, W. Wang⁵⁴, W. H. Wang⁷¹, W. P. Wang^{66,53}, X. Wang^{42,g}, X. F. Wang^{34,j,k}, X. L. Wang^{10,f}, Y. Wang⁵⁶, Y. D. Wang⁴¹, Y. F. Wang^{1,53,58}, Y. H. Wang⁴³, Y. Q. Wang¹, Yaqian Wang^{16,1}, Z. Wang^{1,53}, Z. Y. Wang^{1,58}, Ziyi Wang⁵⁸, D. H. Wei¹³, F. Weidner⁶³, S. P. Wen¹, D. J. White⁶², U. Wiedner⁴, G. Wilkinson⁶⁴, M. Wolke⁷⁰, L. Wollenberg⁴, J. F. Wu^{1,58}, L. H. Wu¹, L. J. Wu^{1,58}, X. Wu^{10,f}, X. H. Wu³⁰, Y. Wu⁶⁶, Z. Wu^{1,53}, L. Xia^{66,53}, T. Xiang^{42,g}, D. Xiao^{34,j,k}, G. Y. Xiao³⁸, H. Xiao^{10,f}, S. Y. Xiao¹, Y. L. Xiao^{10,f}, Z. J. Xiao³⁷, C. Xie³⁸, X. H. Xie^{42,g}, Y. Xie⁴⁵, Y. G. Xie^{1,53}, Y. H. Xie⁶, Z. P. Xie^{66,53}, T. Y. Xing^{1,58}, C. F. Xu¹, C. J. Xu⁵⁴,

G. F. Xu¹, H. Y. Xu⁶¹, Q. J. Xu¹⁵, X. P. Xu⁵⁰, Y. C. Xu⁵⁸, Z. P. Xu³⁸, F. Yan^{10,f}, L. Yan^{10,f}, W. B. Yan^{66,53}, W. C. Yan⁷⁵,
H. J. Yang^{46,e}, H. L. Yang³⁰, H. X. Yang¹, L. Yang⁴⁷, S. L. Yang⁵⁸, Tao Yang¹, Y. F. Yang³⁹, Y. X. Yang^{1,58}, Yifan Yang^{1,58},
M. Ye^{1,53}, M. H. Ye⁸, J. H. Yin¹, Z. Y. You⁵⁴, B. X. Yu^{1,53,58}, C. X. Yu³⁹, G. Yu^{1,58}, T. Yu⁶⁷, X. D. Yu^{42,g}, C. Z. Yuan^{1,58},
L. Yuan², S. C. Yuan¹, X. Q. Yuan¹, Y. Yuan^{1,58}, Z. Y. Yuan⁵⁴, C. X. Yue³⁵, A. A. Zafar⁶⁸, F. R. Zeng⁴⁵, X. Zeng Zeng⁶,
Y. Zeng^{23,h}, Y. H. Zhan⁵⁴, A. Q. Zhang¹, B. L. Zhang¹, B. X. Zhang¹, D. H. Zhang³⁹, G. Y. Zhang¹⁸, H. Zhang⁶⁶,
H. H. Zhang³⁰, H. H. Zhang⁵⁴, H. Y. Zhang^{1,53}, J. L. Zhang⁷², J. Q. Zhang³⁷, J. W. Zhang^{1,53,58}, J. X. Zhang^{34,j,k}, J. Y. Zhang¹,
J. Z. Zhang^{1,58}, Jianyu Zhang^{1,58}, Jiawei Zhang^{1,58}, L. M. Zhang⁵⁶, L. Q. Zhang⁵⁴, Lei Zhang³⁸, P. Zhang¹, Q. Y. Zhang^{35,75},
Shuihan Zhang^{1,58}, Shulei Zhang^{23,h}, X. D. Zhang⁴¹, X. M. Zhang¹, X. Y. Zhang⁴⁵, X. Y. Zhang⁵⁰, Y. Zhang⁶⁴, Y. T. Zhang⁷⁵,
Y. H. Zhang^{1,53}, Yan Zhang^{66,53}, Yao Zhang¹, Z. H. Zhang¹, Z. Y. Zhang⁷¹, Z. Y. Zhang³⁹, G. Zhao¹, J. Zhao³⁵, J. Y. Zhao^{1,58},
J. Z. Zhao^{1,53}, Lei Zhao^{66,53}, Ling Zhao¹, M. G. Zhao³⁹, Q. Zhao¹, S. J. Zhao⁷⁵, Y. B. Zhao^{1,53}, Y. X. Zhao^{28,58},
Z. G. Zhao^{66,53}, A. Zhemchugov^{32,a}, B. Zheng⁶⁷, J. P. Zheng^{1,53}, Y. H. Zheng⁵⁸, B. Zhong³⁷, C. Zhong⁶⁷, X. Zhong⁵⁴, H.
Zhou⁴⁵, L. P. Zhou^{1,58}, X. Zhou⁷¹, X. K. Zhou⁵⁸, X. R. Zhou^{66,53}, X. Y. Zhou³⁵, Y. Z. Zhou^{10,f}, J. Zhu³⁹, K. Zhu¹,
K. J. Zhu^{1,53,58}, L. X. Zhu⁵⁸, S. H. Zhu⁶⁵, S. Q. Zhu³⁸, T. J. Zhu⁷², W. J. Zhu^{10,f}, Y. C. Zhu^{66,53}, Z. A. Zhu^{1,58}, B. S. Zou¹,
J. H. Zou¹

(BESIII Collaboration)

- ¹ Institute of High Energy Physics, Beijing 100049, People's Republic of China
- ² Beihang University, Beijing 100191, People's Republic of China
- ³ Beijing Institute of Petrochemical Technology, Beijing 102617, People's Republic of China
- ⁴ Bochum Ruhr-University, D-44780 Bochum, Germany
- ⁵ Carnegie Mellon University, Pittsburgh, Pennsylvania 15213, USA
- ⁶ Central China Normal University, Wuhan 430079, People's Republic of China
- ⁷ Central South University, Changsha 410083, People's Republic of China
- ⁸ China Center of Advanced Science and Technology, Beijing 100190, People's Republic of China
- ⁹ COMSATS University Islamabad, Lahore Campus, Defence Road, Off Raiwind Road, 54000 Lahore, Pakistan
- ¹⁰ Fudan University, Shanghai 200433, People's Republic of China
- ¹¹ G.I. Budker Institute of Nuclear Physics SB RAS (BINP), Novosibirsk 630090, Russia
- ¹² GSI Helmholtzcentre for Heavy Ion Research GmbH, D-64291 Darmstadt, Germany
- ¹³ Guangxi Normal University, Guilin 541004, People's Republic of China
- ¹⁴ Guangxi University, Nanning 530004, People's Republic of China
- ¹⁵ Hangzhou Normal University, Hangzhou 310036, People's Republic of China
- ¹⁶ Hebei University, Baoding 071002, People's Republic of China
- ¹⁷ Helmholtz Institute Mainz, Staudinger Weg 18, D-55099 Mainz, Germany
- ¹⁸ Henan Normal University, Xinxiang 453007, People's Republic of China
- ¹⁹ Henan University of Science and Technology, Luoyang 471003, People's Republic of China
- ²⁰ Henan University of Technology, Zhengzhou 450001, People's Republic of China
- ²¹ Huangshan College, Huangshan 245000, People's Republic of China
- ²² Hunan Normal University, Changsha 410081, People's Republic of China
- ²³ Hunan University, Changsha 410082, People's Republic of China
- ²⁴ Indian Institute of Technology Madras, Chennai 600036, India
- ²⁵ Indiana University, Bloomington, Indiana 47405, USA
- ²⁶ INFN Laboratori Nazionali di Frascati, (A)INFN Laboratori Nazionali di Frascati, I-00044, Frascati, Italy; (B)INFN Sezione di Perugia, I-06100, Perugia, Italy; (C)University of Perugia, I-06100, Perugia, Italy
- ²⁷ INFN Sezione di Ferrara, (A)INFN Sezione di Ferrara, I-44122, Ferrara, Italy; (B)University of Ferrara, I-44122, Ferrara, Italy
- ²⁸ Institute of Modern Physics, Lanzhou 730000, People's Republic of China
- ²⁹ Institute of Physics and Technology, Peace Avenue 54B, Ulaanbaatar 13330, Mongolia
- ³⁰ Jilin University, Changchun 130012, People's Republic of China
- ³¹ Johannes Gutenberg University of Mainz, Johann-Joachim-Becher-Weg 45, D-55099 Mainz, Germany
- ³² Joint Institute for Nuclear Research, 141980 Dubna, Moscow region, Russia
- ³³ Justus-Liebig-Universitaet Giessen, II. Physikalisches Institut, Heinrich-Buff-Ring 16, D-35392 Giessen, Germany
- ³⁴ Lanzhou University, Lanzhou 730000, People's Republic of China
- ³⁵ Liaoning Normal University, Dalian 116029, People's Republic of China
- ³⁶ Liaoning University, Shenyang 110036, People's Republic of China
- ³⁷ Nanjing Normal University, Nanjing 210023, People's Republic of China
- ³⁸ Nanjing University, Nanjing 210093, People's Republic of China

- ³⁹ Nankai University, Tianjin 300071, People's Republic of China
- ⁴⁰ National Centre for Nuclear Research, Warsaw 02-093, Poland
- ⁴¹ North China Electric Power University, Beijing 102206, People's Republic of China
- ⁴² Peking University, Beijing 100871, People's Republic of China
- ⁴³ Qufu Normal University, Qufu 273165, People's Republic of China
- ⁴⁴ Shandong Normal University, Jinan 250014, People's Republic of China
- ⁴⁵ Shandong University, Jinan 250100, People's Republic of China
- ⁴⁶ Shanghai Jiao Tong University, Shanghai 200240, People's Republic of China
- ⁴⁷ Shanxi Normal University, Linfen 041004, People's Republic of China
- ⁴⁸ Shanxi University, Taiyuan 030006, People's Republic of China
- ⁴⁹ Sichuan University, Chengdu 610064, People's Republic of China
- ⁵⁰ Soochow University, Suzhou 215006, People's Republic of China
- ⁵¹ South China Normal University, Guangzhou 510006, People's Republic of China
- ⁵² Southeast University, Nanjing 211100, People's Republic of China
- ⁵³ State Key Laboratory of Particle Detection and Electronics, Beijing 100049, Hefei 230026, People's Republic of China
- ⁵⁴ Sun Yat-Sen University, Guangzhou 510275, People's Republic of China
- ⁵⁵ Suranaree University of Technology, University Avenue 111, Nakhon Ratchasima 30000, Thailand
- ⁵⁶ Tsinghua University, Beijing 100084, People's Republic of China
- ⁵⁷ Turkish Accelerator Center Particle Factory Group, (A)Istinye University, 34010, Istanbul, Turkey; (B)Near East University, Nicosia, North Cyprus, Mersin 10, Turkey
- ⁵⁸ University of Chinese Academy of Sciences, Beijing 100049, People's Republic of China
- ⁵⁹ University of Groningen, NL-9747 AA Groningen, The Netherlands
- ⁶⁰ University of Hawaii, Honolulu, Hawaii 96822, USA
- ⁶¹ University of Jinan, Jinan 250022, People's Republic of China
- ⁶² University of Manchester, Oxford Road, Manchester, M13 9PL, United Kingdom
- ⁶³ University of Muenster, Wilhelm-Klemm-Strasse 9, 48149 Muenster, Germany
- ⁶⁴ University of Oxford, Keble Road, Oxford OX13RH, United Kingdom
- ⁶⁵ University of Science and Technology Liaoning, Anshan 114051, People's Republic of China
- ⁶⁶ University of Science and Technology of China, Hefei 230026, People's Republic of China
- ⁶⁷ University of South China, Hengyang 421001, People's Republic of China
- ⁶⁸ University of the Punjab, Lahore-54590, Pakistan
- ⁶⁹ University of Turin and INFN, (A)University of Turin, I-10125, Turin, Italy; (B)University of Eastern Piedmont, I-15121, Alessandria, Italy; (C)INFN, I-10125, Turin, Italy
- ⁷⁰ Uppsala University, Box 516, SE-75120 Uppsala, Sweden
- ⁷¹ Wuhan University, Wuhan 430072, People's Republic of China
- ⁷² Xinyang Normal University, Xinyang 464000, People's Republic of China
- ⁷³ Yunnan University, Kunming 650500, People's Republic of China
- ⁷⁴ Zhejiang University, Hangzhou 310027, People's Republic of China
- ⁷⁵ Zhengzhou University, Zhengzhou 450001, People's Republic of China
- ^a Also at the Moscow Institute of Physics and Technology, Moscow 141700, Russia
- ^b Also at the Novosibirsk State University, Novosibirsk, 630090, Russia
- ^c Also at the NRC "Kurchatov Institute", PNPI, 188300, Gatchina, Russia
- ^d Also at Goethe University Frankfurt, 60323 Frankfurt am Main, Germany
- ^e Also at Key Laboratory for Particle Physics, Astrophysics and Cosmology, Ministry of Education; Shanghai Key Laboratory for Particle Physics and Cosmology; Institute of Nuclear and Particle Physics, Shanghai 200240, People's Republic of China
- ^f Also at Key Laboratory of Nuclear Physics and Ion-beam Application (MOE) and Institute of Modern Physics, Fudan University, Shanghai 200443, People's Republic of China
- ^g Also at State Key Laboratory of Nuclear Physics and Technology, Peking University, Beijing 100871, People's Republic of China
- ^h Also at School of Physics and Electronics, Hunan University, Changsha 410082, China
- ⁱ Also at Guangdong Provincial Key Laboratory of Nuclear Science, Institute of Quantum Matter, South China Normal University, Guangzhou 510006, China
- ^j Also at Frontiers Science Center for Rare Isotopes, Lanzhou University, Lanzhou 730000, People's Republic of China
- ^k Also at Lanzhou Center for Theoretical Physics, Lanzhou University, Lanzhou 730000, People's Republic of China
- ^l Also at the Department of Mathematical Sciences, IBA, Karachi, Pakistan

Abstract

Using e^+e^- annihilation data sets collected with the BESIII detector, we measure the cross sections of the processes $e^+e^- \rightarrow e^+e^-$ and $e^+e^- \rightarrow \mu^+\mu^-$ at fifteen center-of-mass energy points in the vicinity of the J/ψ resonance. By a simultaneous fit to the measured, center-of-mass energy dependent cross sections of the two processes, the combined quantities $\Gamma_{ee}\Gamma_{ee}/\Gamma_{\text{tot}}$ and $\Gamma_{ee}\Gamma_{\mu\mu}/\Gamma_{\text{tot}}$ are determined to be (0.346 ± 0.009) and (0.335 ± 0.006) keV, respectively, where Γ_{ee} , $\Gamma_{\mu\mu}$, and Γ_{tot} are the electronic, muonic, and total decay widths of the J/ψ resonance, respectively. Using the resultant $\Gamma_{ee}\Gamma_{ee}/\Gamma_{\text{tot}}$ and $\Gamma_{ee}\Gamma_{\mu\mu}/\Gamma_{\text{tot}}$, the ratio $\Gamma_{ee}/\Gamma_{\mu\mu}$ is calculated to be 1.031 ± 0.015 , which is consistent with the expectation of lepton universality within about two standard deviations. Assuming lepton universality and using the branching fraction of the J/ψ leptonic decay measured by BESIII in 2013, Γ_{tot} and Γ_{ll} are determined to be (93.0 ± 2.1) and (5.56 ± 0.11) keV, respectively, where Γ_{ll} is the average leptonic decay width of the J/ψ resonance.

Keywords: J/ψ , decay width, lepton universality, energy scan, BESIII

1. Introduction

The total and electronic decay widths Γ_{tot} and Γ_{ee} of the J/ψ resonance, present in the Breit-Wigner formulae for all the decay modes of J/ψ produced in e^+e^- collisions [1], are among its most important parameters. Theoretically, these decay widths, reflecting J/ψ internal interactions, are predicted by various potential models [2–6] and lattice quantum chromodynamics [7]. Measurements of these decay widths and comparisons of the experimental results with different theoretical calculations can help us gain a better understanding of the underlying physics.

Furthermore, the ratio of the electronic to muonic decay widths of the J/ψ resonance, $\Gamma_{ee}/\Gamma_{\mu\mu}$, can be used to test the lepton universality assumption [8]. Based on the assumption, the ratio is derived to be [9]

$$\Gamma_{ee}/\Gamma_{\mu\mu} = \frac{\beta_e(3 - \beta_e^2)}{\beta_\mu(3 - \beta_\mu^2)}, \quad (1)$$

with

$$\beta_l = \sqrt{1 - (2m_l/M)^2} \quad l = e, \mu, \quad (2)$$

where m_e , m_μ , and M are the masses of electron, muon, and the J/ψ resonance, respectively. Taking the values of m_e , m_μ , and M from the Particle Data Group (PDG) [1], $\Gamma_{ee}/\Gamma_{\mu\mu}$ is calculated to be 1.00000814211(6), which has a deviation from 1 that is far less than the experimental precision at present. Thus, any observed, significant deviation of $\Gamma_{ee}/\Gamma_{\mu\mu}$ from 1 will be a hint of physics beyond the Standard Model [10].

Since the discovery of the J/ψ resonance in 1974 [11, 12], its decay widths have been measured by many experiments [13–17]. The precision of the

measurements has been improved significantly in the past two decades. In 2004 and 2006, the J/ψ decay widths have been measured by studying the J/ψ samples produced in the initial state radiation (ISR) return process $e^+e^- \rightarrow \gamma^{\text{ISR}}\mu^+\mu^-$ collected at the $\Upsilon(4S)$ and $\psi(3770)$ peaks by BaBar [18] and CLEO [19], respectively. In 2010, KEDR improved the measurement precision by performing an energy scan (ES) around the J/ψ peak and studying the J/ψ production in the processes $e^+e^- \rightarrow e^+e^-$ and $e^+e^- \rightarrow \mu^+\mu^-$ [20]. In 2018 and 2020, KEDR presented new results with the J/ψ production in the processes $e^+e^- \rightarrow e^+e^-$ and $e^+e^- \rightarrow$ inclusive hadrons [21].

Operating in the τ -charm energy region, the high luminosity of the BEPCII collider [22] and the excellent performance of the BESIII detector [23] offer us a good opportunity for the precision measurements of the J/ψ decay widths. In 2016, BESIII measured the J/ψ decay widths by applying the ISR return technique to the data sample collected at the $\psi(3770)$ peak, and obtained a result with improved precision [24]. In this Letter, we report a new precision measurement of the J/ψ decay widths with the ES method, confirming and complementing the above measurement.

Since the J/ψ resonance contributes to the vacuum polarization in the time-like region, the cross sections of the processes $e^+e^- \rightarrow e^+e^-$ and $e^+e^- \rightarrow \mu^+\mu^-$ are functions of the J/ψ decay widths [25, 26]. Specifically, the cross section (σ_0) of each process with respect to the center-of-mass (CM) energy (W_0) can be written as

$$\sigma_0(W_0) = \sigma_0^{\text{C}}(W_0) + \sigma_0^{\text{R}}(W_0) + \sigma_0^{\text{I}}(W_0), \quad (3)$$

where σ_0^{C} , σ_0^{R} and σ_0^{I} are the continuum, resonance and interference terms, respectively. The formula still

holds after considering the ISR effect, and we take σ_0 , σ_0^C , σ_0^R and σ_0^I here as the quantities with ISR considered. Unlike the term σ_0^C , the terms σ_0^R and σ_0^I depend on the J/ψ decay widths, and their analytic forms are derived in Ref. [27] using the structure function method [28, 29].

In Eq. (3), σ_0^R is the primary term related to the J/ψ decay widths, and its major subterm is proportional to $\Gamma_{ee}\Gamma_{ee}/\Gamma_{\text{tot}}$ and $\Gamma_{ee}\Gamma_{\mu\mu}/\Gamma_{\text{tot}}$ for the processes $e^+e^- \rightarrow e^+e^-$ and $e^+e^- \rightarrow \mu^+\mu^-$, respectively [27]. Therefore, we can determine $\Gamma_{ee}\Gamma_{ee}/\Gamma_{\text{tot}}$ and $\Gamma_{ee}\Gamma_{\mu\mu}/\Gamma_{\text{tot}}$ by fitting to the measured, CM energy dependent cross sections of the two processes. Then, $\Gamma_{ee}/\Gamma_{\mu\mu}$ can be evaluated as the ratio of $\Gamma_{ee}\Gamma_{ee}/\Gamma_{\text{tot}}$ to $\Gamma_{ee}\Gamma_{\mu\mu}/\Gamma_{\text{tot}}$. Combined with the branching fraction of the J/ψ leptonic decay measured by BESIII in 2013 [30], the total and leptonic J/ψ decay widths can be obtained from $\Gamma_{ee}\Gamma_{ee}/\Gamma_{\text{tot}}$ and $\Gamma_{ee}\Gamma_{\mu\mu}/\Gamma_{\text{tot}}$ as well.

2. Experimental facilities and data sets

The data used in this work were collected with the BESIII detector [23], which operates at the south crossing point of the BEPCII collider [22]. BEPCII is a double-ring e^+e^- collider operating in the τ -charm energy region (2.0-4.9 GeV) with its achieved peak luminosity of $10^{33} \text{ cm}^{-2}\text{s}^{-1}$ at the CM energy $\sqrt{s} = 3.773$

GeV. The BESIII detector with a geometrical acceptance of 93% of 4π , consists of the following main components: (1) a small-cell, helium-based main drift chamber (MDC) measuring the momenta of charged tracks in a 1 T magnetic field with a resolution of 0.5% for 1 GeV/c transverse momentum and the specific energy loss (dE/dx) with a resolution of 6%; (2) a time-of-flight (TOF) system for particle identification composed of a barrel and two endcaps made of plastic scintillators; the time resolution is 80 ps in the barrel, and 110 ps in the endcaps; (3) an electromagnetic calorimeter (EMC) made of CsI(Tl) crystals arranged in a cylindrical shape (barrel) and two endcaps; for 1.0 GeV photons, the energy resolution is 2.5% in the barrel and 5% in the endcaps; (4) a superconducting solenoid magnet providing a nominal magnetic field of 1 T (0.9 T in 2012) parallel to the beam direction; (5) a muon chamber system made of resistive plate chambers with position resolution about 2 cm.

In addition, a beam energy measurement system (BEMS), located at the north crossing point of the BEPCII storage rings, is used to determine the BEPCII beam energies by measuring the energies of Compton back-scattered photons [31].

In 2012, an ES experiment was performed at fifteen CM energy points in the vicinity of the J/ψ resonance. The measured CM energies and integrated luminosities are summarized in Table 1. The CM energies are

Table 1: Basic information of the data samples at all individual CM energy points, including the proposed CM energies (Prop. \sqrt{s}) before the data taking, the CM energies measured by the BEMS and calibrated with the J/ψ mass from the PDG (Calib. BEMS \sqrt{s}), and the integrated luminosities (Int. L). For Calib. BEMS \sqrt{s} and Int. L , the first uncertainties are statistical and the second ones are systematic.

Prop. \sqrt{s} (MeV)	Calib. BEMS \sqrt{s} (MeV)	Int. L (pb^{-1})
3050.0	$3049.642 \pm 0.026 \pm 0.033$	$14.919 \pm 0.029 \pm 0.158$
3060.0	$3058.693 \pm 0.028 \pm 0.033$	$15.060 \pm 0.029 \pm 0.158$
3083.0	$3082.496 \pm 0.023 \pm 0.033$	$4.769 \pm 0.017 \pm 0.052$
3090.0	$3088.854 \pm 0.022 \pm 0.033$	$15.558 \pm 0.030 \pm 0.162$
3093.0	$3091.760 \pm 0.025 \pm 0.033$	$14.910 \pm 0.030 \pm 0.157$
3094.3	$3094.697 \pm 0.084 \pm 0.033$	$2.143 \pm 0.011 \pm 0.023$
3095.2	$3095.430 \pm 0.081 \pm 0.033$	$1.816 \pm 0.010 \pm 0.019$
3095.8	$3095.826 \pm 0.075 \pm 0.033$	$2.135 \pm 0.011 \pm 0.023$
3096.9	$3097.213 \pm 0.076 \pm 0.033$	$2.069 \pm 0.011 \pm 0.024$
3098.2	$3098.340 \pm 0.075 \pm 0.033$	$2.203 \pm 0.011 \pm 0.023$
3099.0	$3099.042 \pm 0.093 \pm 0.033$	$0.756 \pm 0.007 \pm 0.008$
3101.5	$3101.359 \pm 0.106 \pm 0.033$	$1.612 \pm 0.010 \pm 0.018$
3105.5	$3105.580 \pm 0.090 \pm 0.033$	$2.106 \pm 0.011 \pm 0.022$
3112.0	$3112.051 \pm 0.093 \pm 0.033$	$1.720 \pm 0.010 \pm 0.019$
3120.0	$3119.878 \pm 0.115 \pm 0.033$	$1.264 \pm 0.009 \pm 0.013$

measured by the BEMS and calibrated according to the J/ψ mass value given by the PDG [1]. As a consequence, the J/ψ mass can not be determined in this work. The CM energy calibration process fits to the J/ψ lineshapes in the e^+e^- and $\mu^+\mu^-$ final states simultaneously to their preliminary measured, CM energy dependent cross sections. Adding the uncertainties of the J/ψ masses from the fit and from the PDG in quadrature gives a total calibration uncertainty of 0.033 MeV, which is comparable with the systematic uncertainty (0.043 MeV) of the calibration (via the inclusive hadronic decay mode) to the small J/ψ scan data used for the τ mass measurement [32]. The corresponding integrated luminosities are measured offline with $e^+e^- \rightarrow \gamma\gamma$ events [33].

To determine the signal detection efficiencies, Monte Carlo (MC) simulated events of the processes $e^+e^- \rightarrow e^+e^-$ and $e^+e^- \rightarrow \mu^+\mu^-$ in the polar angle ranges of 34° - 146° and 0° - 180° , respectively, incorporating the ISR and final state radiation (FSR) effects, are simulated with a revised version of the BABAYAGA-3.5 [34] generator, which is modified by the authors to explicitly involve the J/ψ resonance in the vacuum polarization. In addition, MC events of the processes $e^+e^- \rightarrow$ inclusive hadrons and $\gamma^*\gamma^* \rightarrow X$ ($e^+e^-e^+e^-$, $e^+e^-\mu^+\mu^-$, etc.) are generated for background studies with the CONEXC [35] and BESTWOGAM [36] generators, respectively. When generating these events, the calibrated BEMS CM energies are used.

A GEANT4 [37] based MC simulation program including the geometric description and response of the detector is used to simulate the interaction of final state particles in the detector. Both the experimental data and simulated MC are reconstructed and analysed under the GAUDI [38] based offline software system.

3. Event selection

The signal candidates of $e^+e^- \rightarrow e^+e^-$ and $e^+e^- \rightarrow \mu^+\mu^-$ events are required to have two oppositely charged tracks in the MDC. Each charged track has to fulfill the following requirements: it must originate from the interaction region of $|V_r| < 1$ cm and $|V_z| < 10$ cm, where $|V_r|$ and $|V_z|$ are its closest approach relative to the collision point in the x-y plane and along the z axis (taken as the axis of the MDC), respectively; it must hit the detector in the barrel region of $|\cos\theta| < 0.8$, where θ is the polar angle of the reconstructed momentum vector with respect to the z axis.

For $e^+e^- \rightarrow e^+e^-$ candidates, the next two criteria are applied further to each of the selected tracks: its momentum (P) is required to be larger than 0.7 times the

beam energy (E_{beam}), and its energy deposited in the EMC (E) has to be larger than 0.6 times the momentum.

For $e^+e^- \rightarrow \mu^+\mu^-$ candidates, the following conditions are required in addition: for each of the selected tracks, P must be larger than $0.8E_{\text{beam}}$, E has to be larger than 25 MeV and less than $0.25P$, and valid timing information is required to be left in the TOF; at the event level, no neutral showers with a deposited energy above 25 MeV are allowed in the EMC, and the difference of the flight time of the two charged tracks ($\Delta t_{\text{TOF}}^\mu$) obtained with the TOF has to be less than 1.5 ns to suppress cosmic rays.

Figure 1 shows the comparison between data and MC simulation of variables used in the event selection. The data shown in the figure are those of surviving candidate events subtracting the residual background estimated with the MC simulation. In general, the MC simulation provides a good description of the data although minor discrepancies between them are visible. The effects of these discrepancies are taken into account in the systematic uncertainty estimation (see Section 4.2 for details).

For the process $e^+e^- \rightarrow e^+e^- (\mu^+\mu^-)$, the efficiencies obtained from the signal MC samples are about 70% (80%), and the background levels estimated with the MC simulation are less than 0.05% (0.5%). Closer examination with a generic event type analysis tool, TOPOANA [39], shows that the backgrounds mainly arise from events with $\pi^+\pi^-$, K^+K^- or $e^+e^-e^+e^-$ ($e^+e^-\mu^+\mu^-$) final states.

4. Cross section measurement

4.1. Nominal results with statistical uncertainties

Usually, the cross section σ is determined from

$$\sigma = \frac{N_{\text{sig}} - N_{\text{bkgs}}}{L \cdot \epsilon_{\text{trg}} \cdot \epsilon_{\text{reysel}}} \cdot f, \quad (4)$$

where N_{sig} is the number of signal events selected from data, N_{bkgs} is the number of the residual background events, L is the integrated luminosity, ϵ_{trg} is the trigger efficiency, ϵ_{reysel} is the reconstruction-selection efficiency and f is a reconstruction efficiency correction factor.

The trigger efficiency is taken as 100% in this work [40]. The correction factor f is related to the imperfection of the detector simulation. In practice, the reconstruction efficiencies (including the tracking efficiency in the MDC and the cluster reconstruction efficiency in the EMC) from MC simulation deviate those from data. We study the corresponding reconstruction

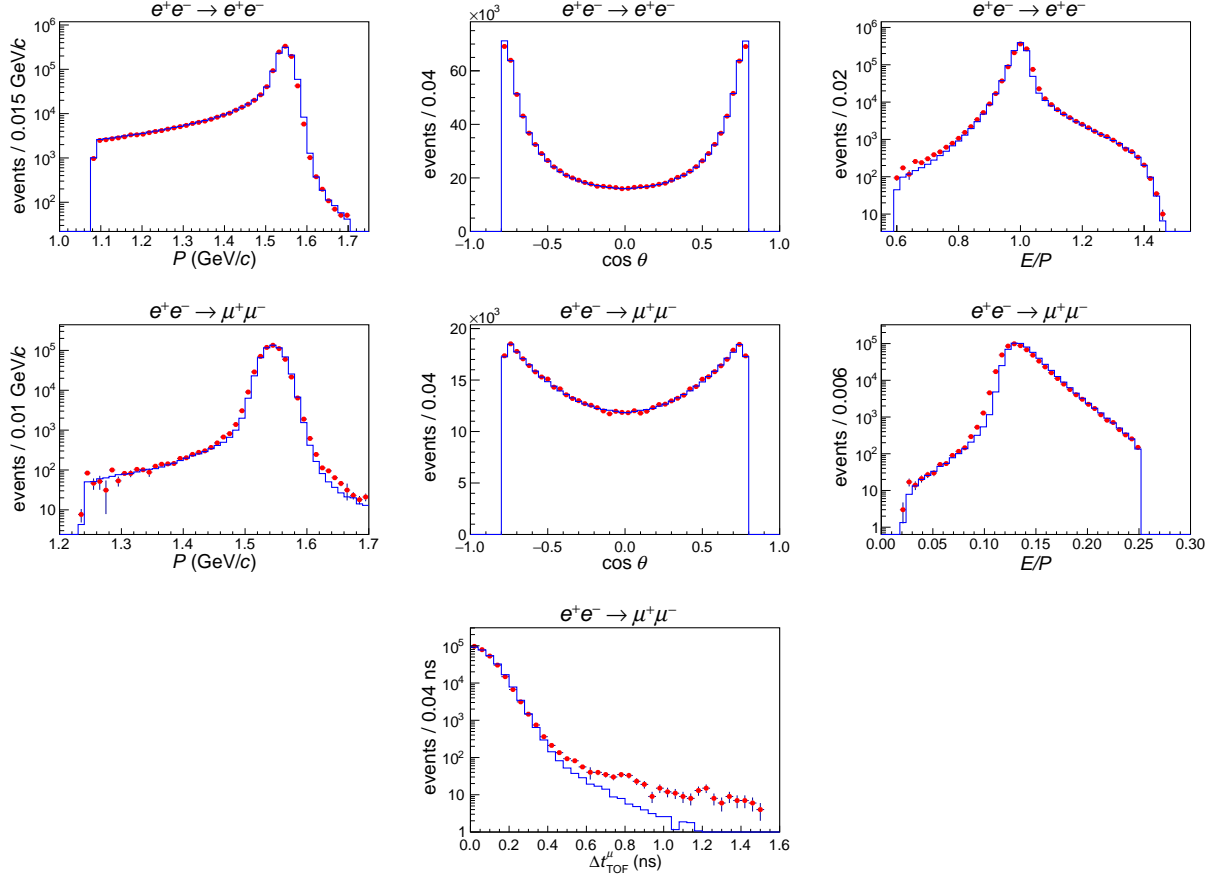


Fig. 1: Comparison between data and MC simulation of the distributions of the variables used in the selection criteria for the processes $e^+e^- \rightarrow e^+e^-$ and $e^+e^- \rightarrow \mu^+\mu^-$ at $\sqrt{s} = 3096.9$ MeV. For all the plots, dots with error bars show the background-subtracted data (the background level is evaluated with the MC simulation) and the histograms denote the signal MC. The small discrepancy in the last plot is due to the imperfection of the MC simulation, and it has a negligible effect on the cross section measurement of $e^+e^- \rightarrow \mu^+\mu^-$.

efficiencies for leptons in different $\cos \theta$ bins. To compensate the deviation of the reconstruction-selection efficiency, the correction factor f is introduced as

$$f = N_{\text{obs}}^{\text{MC}} / \left(\sum_m \sum_n N_{\text{obs}}^{\text{MC}}(m, n) \cdot \frac{\epsilon_{\text{trk}}^{\text{data}}(m)}{\epsilon_{\text{trk}}^{\text{MC}}(m)} \cdot \frac{\epsilon_{\text{trk}}^{\text{data}}(n)}{\epsilon_{\text{trk}}^{\text{MC}}(n)} \cdot \frac{\epsilon_{\text{clst}}^{\text{data}}(m)}{\epsilon_{\text{clst}}^{\text{MC}}(m)} \cdot \frac{\epsilon_{\text{clst}}^{\text{data}}(n)}{\epsilon_{\text{clst}}^{\text{MC}}(n)} \right). \quad (5)$$

Here, $N_{\text{obs}}^{\text{MC}}$ stands for the number of surviving events of signal MC samples, m (n) for the m^{th} (n^{th}) $\cos \theta$ bin of positively (negatively) charged leptons, $\epsilon_{\text{trk}}^{\text{data}}$ and $\epsilon_{\text{trk}}^{\text{MC}}$ ($\epsilon_{\text{clst}}^{\text{data}}$ and $\epsilon_{\text{clst}}^{\text{MC}}$) for the MDC tracking efficiency (EMC cluster reconstruction efficiency) of leptons from data and MC simulation, respectively.

The measured cross sections and related input quantities at all individual CM energy points of the processes $e^+e^- \rightarrow e^+e^-$ and $e^+e^- \rightarrow \mu^+\mu^-$ are summarized in Tables 2 and 3, respectively.

4.2. Systematic uncertainties

The systematic uncertainties of the measured cross sections arise mainly from the integrated luminosities, trigger efficiencies, CM energies, reconstruction and selection efficiencies, efficiency correction factors and residual backgrounds.

The uncertainties due to the integrated luminosities are estimated to be less than 1.40% (1.26% at $\sqrt{s} = 3096.9$ MeV) [33], while those resulting from trigger efficiencies are evaluated as 0.10% [40].

Table 2: Measured cross sections and related input quantities of the process $e^+e^- \rightarrow e^+e^-$ at all individual CM energy points. The uncertainties of the input quantities are statistical, while the first and second uncertainties of cross sections are statistical and systematic, respectively. Notably, the cross sections here are confined in the polar angle range of 34° – 146° .

Prop. \sqrt{s} (MeV)	N_{sig}	N_{bkgs}	$\epsilon_{\text{recesel}}$	f	σ (nb)
3.0500	2274639 ± 1508	164 ± 13	0.6909 ± 0.0002	0.9989 ± 0.0002	$220.4 \pm 0.2 \pm 2.5$
3.0600	2286953 ± 1512	145 ± 12	0.6910 ± 0.0002	0.9989 ± 0.0002	$219.5 \pm 0.2 \pm 2.5$
3.0830	710011 ± 843	57 ± 8	0.6913 ± 0.0002	0.9989 ± 0.0002	$215.1 \pm 0.3 \pm 2.6$
3.0900	2341309 ± 1530	182 ± 13	0.6918 ± 0.0002	0.9989 ± 0.0002	$217.3 \pm 0.2 \pm 2.4$
3.0930	2240003 ± 1497	181 ± 13	0.6918 ± 0.0002	0.9989 ± 0.0002	$216.9 \pm 0.2 \pm 2.5$
3.0943	345449 ± 588	34 ± 6	0.6989 ± 0.0002	0.9990 ± 0.0002	$230.4 \pm 0.4 \pm 2.9$
3.0952	335948 ± 580	52 ± 7	0.7180 ± 0.0002	0.9991 ± 0.0002	$257.3 \pm 0.4 \pm 3.4$
3.0958	487256 ± 698	61 ± 8	0.7329 ± 0.0002	0.9992 ± 0.0002	$311.2 \pm 0.4 \pm 6.9$
3.0969	577995 ± 760	174 ± 13	0.7580 ± 0.0002	0.9994 ± 0.0002	$368.2 \pm 0.5 \pm 5.2$
3.0982	443694 ± 666	104 ± 10	0.7286 ± 0.0002	0.9992 ± 0.0002	$276.2 \pm 0.4 \pm 4.2$
3.0990	127932 ± 358	19 ± 4	0.7082 ± 0.0002	0.9991 ± 0.0002	$238.6 \pm 0.7 \pm 4.3$
3.1015	242275 ± 492	26 ± 5	0.6958 ± 0.0002	0.9990 ± 0.0002	$215.7 \pm 0.4 \pm 2.8$
3.1055	313080 ± 560	32 ± 6	0.6929 ± 0.0002	0.9990 ± 0.0002	$214.3 \pm 0.4 \pm 2.7$
3.1120	251731 ± 502	21 ± 5	0.6919 ± 0.0002	0.9990 ± 0.0002	$211.3 \pm 0.4 \pm 2.8$
3.1200	185572 ± 431	13 ± 4	0.6913 ± 0.0002	0.9990 ± 0.0002	$212.1 \pm 0.5 \pm 2.8$

Table 3: Measured cross sections and related input quantities of the process $e^+e^- \rightarrow \mu^+\mu^-$ at all individual CM energy points. The uncertainties of the input quantities are statistical, while the first and second uncertainties of cross sections are statistical and systematic, respectively. Here, the cross sections are defined in the polar angle range of 0° – 180° .

Prop. \sqrt{s} (MeV)	N_{sig}	N_{bkgs}	$\epsilon_{\text{recesel}}$	f	σ (nb)
3.0500	85997 ± 293	313 ± 18	0.5359 ± 0.0002	1.0094 ± 0.0003	$10.82 \pm 0.04 \pm 0.12$
3.0600	85639 ± 293	316 ± 18	0.5360 ± 0.0002	1.0094 ± 0.0003	$10.67 \pm 0.04 \pm 0.12$
3.0830	24413 ± 156	93 ± 10	0.5286 ± 0.0002	1.0094 ± 0.0003	$9.74 \pm 0.06 \pm 0.12$
3.0900	72967 ± 270	344 ± 19	0.5202 ± 0.0002	1.0094 ± 0.0003	$9.06 \pm 0.03 \pm 0.11$
3.0930	60436 ± 246	336 ± 18	0.5056 ± 0.0002	1.0094 ± 0.0003	$8.05 \pm 0.03 \pm 0.10$
3.0943	17432 ± 132	82 ± 9	0.5781 ± 0.0002	1.0093 ± 0.0003	$14.13 \pm 0.11 \pm 0.35$
3.0952	53866 ± 232	176 ± 13	0.6299 ± 0.0002	1.0093 ± 0.0003	$47.36 \pm 0.20 \pm 0.66$
3.0958	158653 ± 398	318 ± 18	0.6366 ± 0.0002	1.0093 ± 0.0003	$117.59 \pm 0.29 \pm 1.51$
3.0969	287418 ± 536	728 ± 27	0.6418 ± 0.0002	1.0093 ± 0.0003	$217.88 \pm 0.41 \pm 2.81$
3.0982	158804 ± 399	294 ± 17	0.6369 ± 0.0002	1.0093 ± 0.0003	$114.03 \pm 0.29 \pm 1.39$
3.0990	27505 ± 166	58 ± 8	0.6216 ± 0.0002	1.0093 ± 0.0003	$58.92 \pm 0.35 \pm 0.85$
3.1015	23087 ± 152	119 ± 11	0.5981 ± 0.0002	1.0093 ± 0.0003	$24.04 \pm 0.16 \pm 0.36$
3.1055	21595 ± 147	139 ± 12	0.5786 ± 0.0002	1.0093 ± 0.0003	$17.77 \pm 0.12 \pm 0.26$
3.1120	14357 ± 120	69 ± 8	0.5674 ± 0.0002	1.0093 ± 0.0003	$14.78 \pm 0.12 \pm 0.21$
3.1200	9352 ± 97	53 ± 7	0.5570 ± 0.0002	1.0093 ± 0.0003	$13.33 \pm 0.14 \pm 0.19$

To estimate the uncertainties due to the CM energies, two additional sets of MC samples are generated by increasing or decreasing the CM energies by one standard deviation with respect to their nominal values. The largest changes of the efficiencies with respect to their nominal values are taken as the uncertainties.

The uncertainties associated with the momentum requirement for the process $e^+e^- \rightarrow e^+e^-$ are estimated by changing the selection criteria from $P > 0.7E_{\text{beam}}$

to $P > 0.6E_{\text{beam}}$. The resultant changes in the calculated cross sections are taken as the uncertainties. The uncertainties related to other requirements are estimated with the similar method. Specifically, for the selection of $e^+e^- \rightarrow e^+e^-$ events, the analysis is carried out with the alternative criteria of $|\cos\theta| < 0.7$ and $E/P < 0.7$, individually, while for $e^+e^- \rightarrow \mu^+\mu^-$, the analysis is repeated with the alternative criteria of $P > 0.9E_{\text{beam}}$, $|\cos\theta| < 0.7$, $E/P < 0.35$ and $\Delta t_{\text{TOF}}^\mu < 2.5$ ns,

Table 4: Relative systematic uncertainties of the measured cross sections of the processes $e^+e^- \rightarrow e^+e^-$ and $e^+e^- \rightarrow \mu^+\mu^-$ at $\sqrt{s} = 3096.9$ MeV.

Source	Uncertainty (%)	
	$e^+e^- \rightarrow e^+e^-$	$e^+e^- \rightarrow \mu^+\mu^-$
Integrated luminosity measurement	1.26	1.26
Trigger efficiency determination	0.10	0.10
CM energy measurement	0.17	0.11
$\cos \theta$ requirement	0.55	0.01
P requirement	0.13	0.02
E/P requirement	0.05	0.01
$\Delta t_{\text{TOF}}^\mu$ requirement	—	0.05
Efficiency correction factor f	0.10	0.10
Residual backgrounds	0.03	0.25
Total	1.40	1.30

individually.

As shown in Tables 2 and 3, the statistical uncertainties of the efficiency correction factors are 0.02% and 0.03% for the processes $e^+e^- \rightarrow e^+e^-$ and $e^+e^- \rightarrow \mu^+\mu^-$, respectively, which are determined from the statistics of the samples used to study the reconstruction efficiencies. On the other hand, detailed studies show that the purities of the control samples for the electron tracking, electron clustering, muon tracking, and muon clustering efficiencies in data are about 99.99%, 99.81%, 98.45%, and 99.52%, respectively. Considering other factors, such as the background contaminations, the uncertainties resulting from the efficiency correction factors can be roughly and conservatively estimated to be 0.10% for both the $e^+e^- \rightarrow e^+e^-$ and $e^+e^- \rightarrow \mu^+\mu^-$ processes.

The numbers of residual background events, estimated with the MC simulation, are subtracted from the numbers of surviving events in the calculation of the cross sections, and hence the uncertainties of background levels need be taken into account. Since the uncertainties of the cross sections for some dominant background channels (for example, $e^+e^- \rightarrow K^+K^-$) set in the generator are as large as 100%, we therefore take the background levels themselves as the related uncertainties. As a result, the uncertainties for the processes $e^+e^- \rightarrow e^+e^-$ and $e^+e^- \rightarrow \mu^+\mu^-$ at $\sqrt{s} = 3096.9$ MeV are 0.03% and 0.25%, respectively.

Table 4 shows a summary of the systematic uncertainties of the measured cross sections of the processes $e^+e^- \rightarrow e^+e^-$ and $e^+e^- \rightarrow \mu^+\mu^-$ at $\sqrt{s} = 3096.9$

MeV. The total systematic uncertainties, 1.40% and 1.29% for the two processes individually, are the square root of the quadratic sum of the individual uncertainties and dominated by those associated with the integrated luminosities. The systematic uncertainties of the measured cross sections at other CM energy points are estimated with the same method, and they are summarized in Tables 2 and 3 together with the statistical uncertainties.

4.3. Correlation analysis

To consider the correlations between the measured cross sections of the same process at different CM energy points, the corresponding covariance matrices are estimated. To estimate such a covariance matrix, contributions from all related uncertainty sources are analysed and estimated according to their nature and the method of uncertainty propagation. To get an impression of the strength of these correlations, the correlation coefficient matrices of the measured cross sections of the processes $e^+e^- \rightarrow e^+e^-$ and $e^+e^- \rightarrow \mu^+\mu^-$ are shown in Fig. 2. We find that the correlations are strong and can not be neglected.

In the covariance matrix analysis above, the corresponding covariance matrix of the measured luminosities at different CM energy points is estimated in advance with the similar method. This matrix is required when estimating the covariance matrices of the measured cross sections and constructing the global χ^2 function for the simultaneous fit of the processes $e^+e^- \rightarrow e^+e^-$ and $e^+e^- \rightarrow \mu^+\mu^-$ (see Section 5.2).

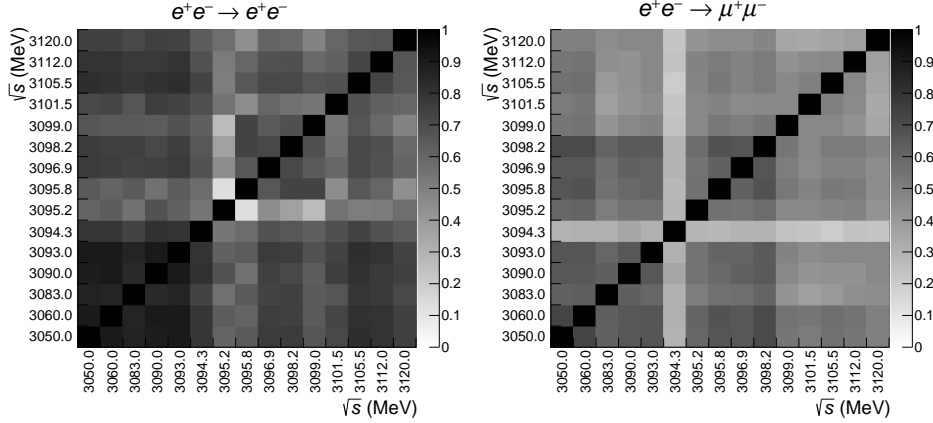


Fig. 2: Correlation coefficient matrices of the measured cross sections of the processes $e^+e^- \rightarrow e^+e^-$ and $e^+e^- \rightarrow \mu^+\mu^-$.

5. Decay width determination

5.1. Energy spread and final state radiation

To determine the J/ψ decay widths, a simultaneous fit to the measured, CM energy dependent cross sections of the processes $e^+e^- \rightarrow e^+e^-$ and $e^+e^- \rightarrow \mu^+\mu^-$ is required. In the theoretical formulae used in the fit, the effects of the beam energy spread and FSR are taken into account as well.

By assuming the CM energy spread follows a Gaussian distribution, the theoretical cross section is

$$\sigma(W) = \int \sigma_0(W_0) \left(\frac{1}{\sqrt{2\pi}S_W} e^{-\frac{(W_0-W)^2}{2S_W^2}} \right) dW_0. \quad (6)$$

Here, W ($= \sqrt{s}$) and S_W are the mean and standard deviation of the CM energy distribution, respectively. According to the formula and the expression of σ_0 in Eq. (3), σ can also be divided into three terms: the continuum term (σ^C), the resonance term (σ^R) and interference term (σ^I). In practice, σ^C is evaluated with the BABAYAGA-3.5 generator [34] with the effects of J/ψ and FSR switched off, while $\sigma^R + \sigma^I$ is calculated using the analytic formulae for $\sigma_0^R + \sigma_0^I$ in Ref. [27].

In Eq. (3), only the ISR effect is involved in σ_0 . To take into account the FSR effect, we introduce a correction factor R^{FSR} into the theoretical cross section:

$$\sigma_0^{\text{theor}}(W) = \sigma(W) \cdot R^{\text{FSR}}(W). \quad (7)$$

In practice, R^{FSR} is obtained with the BABAYAGA-3.5 generator [34] as the ratio of the calculated cross sections with and without the FSR effect. For example, at

$\sqrt{s} = 3096.9$ MeV, R^{FSR} is 0.980 and 0.998 for the processes $e^+e^- \rightarrow e^+e^-$ and $e^+e^- \rightarrow \mu^+\mu^-$, respectively.

Due to the high-order corrections related to the FSR effect, the cross sections of the processes $e^+e^- \rightarrow e^+e^-$ and $e^+e^- \rightarrow \mu^+\mu^-$ are calculated by the BABAYAGA-3.5 generator with the uncertainties of 0.5% and 1.0%, respectively [34]. Thus, systematic deviations of $R^{\text{FSR}}(W)$ from their truth values probably appear in the vicinity of the J/ψ resonance. To take the possible deviations into consideration, we implement one free scaling parameter in the theoretical cross section formula of each process for the simultaneous fit,

$$\sigma^{\text{theor}}(W) = \sigma_0^{\text{theor}}(W) \cdot F. \quad (8)$$

Specifically, the free scaling parameters for the processes $e^+e^- \rightarrow e^+e^-$ and $e^+e^- \rightarrow \mu^+\mu^-$ are referred to as F_{ee} and $F_{\mu\mu}$, respectively.

5.2. Global χ^2 function

To take into account the correlations between the measured cross sections of different processes and/or at different CM energy points, as well as the uncertainties of the CM energies, we construct a global χ^2 function for the simultaneous fit according to the standard covariance matrix method as

$$\chi^2 = \Delta\sigma^T \cdot V^{-1} \cdot \Delta\sigma, \quad (9)$$

where

$$\Delta\sigma(i) = \begin{cases} \sigma_{ee}^{\text{exper}}(i) - \sigma_{ee}^{\text{theor}}(i) & i = 1, 2 \dots 14, 15 \\ \sigma_{\mu\mu}^{\text{exper}}(i - 15) - \sigma_{\mu\mu}^{\text{theor}}(i - 15) & i = 16, 17 \dots 29, 30 \end{cases} \quad (10)$$

and

$$V(i, j) = \begin{cases} V_{ee}(i, j) + \delta(i, j) \left(\frac{\partial \sigma_{ee}^{\text{theor}}}{\partial W}(i) \Delta W(i) \right)^2 & \text{①} \\ \frac{\sigma_{ee}^{\text{exper}}(i) \sigma_{\mu\mu}^{\text{exper}}(j-15)}{L(i) L(j-15)} V_L(i, j-15) + \delta(i, j-15) \frac{\partial \sigma_{ee}^{\text{theor}}}{\partial W}(i) \frac{\partial \sigma_{\mu\mu}^{\text{theor}}}{\partial W}(i) (\Delta W(i))^2 & \text{②} \\ \frac{\sigma_{ee}^{\text{exper}}(j) \sigma_{\mu\mu}^{\text{exper}}(i-15)}{L(i-15) L(j)} V_L(i-15, j) + \delta(i-15, j) \frac{\partial \sigma_{ee}^{\text{theor}}}{\partial W}(j) \frac{\partial \sigma_{\mu\mu}^{\text{theor}}}{\partial W}(j) (\Delta W(j))^2 & \text{③} \\ V_{\mu\mu}(i-15, j-15) + \delta(i-15, j-15) \left(\frac{\partial \sigma_{\mu\mu}^{\text{theor}}}{\partial W}(i-15) \Delta W(i-15) \right)^2 & \text{④} \end{cases} \quad (11)$$

with

$$\begin{cases} \text{① denotes } i = 1, 2 \dots 14, 15, j = 1, 2 \dots 14, 15 \\ \text{② denotes } i = 1, 2 \dots 14, 15, j = 16, 17 \dots 29, 30 \\ \text{③ denotes } i = 16, 17 \dots 29, 30, j = 1, 2 \dots 14, 15 \\ \text{④ denotes } i = 16, 17 \dots 29, 30, j = 16, 17 \dots 29, 30. \end{cases} \quad (12)$$

Here, $\sigma_{ee}^{\text{exper}}$ and $\sigma_{ee}^{\text{theor}}$ ($\sigma_{\mu\mu}^{\text{exper}}$ and $\sigma_{\mu\mu}^{\text{theor}}$) are the experimental measured and theoretical predicted cross sections of the process $e^+e^- \rightarrow e^+e^-$ ($\mu^+\mu^-$), V_{ee} ($V_{\mu\mu}$) is the covariance matrix of the measured cross sections of $e^+e^- \rightarrow e^+e^-$ ($\mu^+\mu^-$), V_L is the covariance matrix of the measured luminosities, i and j are the horizontal and vertical indices of the 30×30 covariance matrix V , δ is Kronecker delta function, and ΔW is the statistical uncertainty of the CM energy as listed in Table 1, whose systematic uncertainty, 0.033 MeV, will be taken into account by examining the changes of the fit result due to the changes of the CM energies by 0.033 MeV.

5.3. Simultaneous fit and parameter transformation

By minimizing the global χ^2 function, the simultaneous fit to the measured, CM energy dependent cross sections of the processes $e^+e^- \rightarrow e^+e^-$ and $e^+e^- \rightarrow \mu^+\mu^-$ is carried out. In the fit, the following six parameters M , $\Gamma_{ee}\Gamma_{ee}/\Gamma_{\text{tot}}$, $\Gamma_{ee}\Gamma_{\mu\mu}/\Gamma_{\text{tot}}$, S_W , F_{ee} and $F_{\mu\mu}$ are float, while $\sigma^C(W)$ and $R^{\text{FSR}}(W)$ are expressed as piecewise linear interpolation functions based on hundreds of pairs of (W, σ^C) and (W, R^{FSR}) values obtained with the BABAYAGA-3.5 generator. The resultant fit curves are shown in Fig. 3, and the corresponding fit quality is $\chi_{\text{min}}^2/ndf \approx 23.0/24 \approx 1.0$, where χ_{min}^2 and ndf are the minimized global chisquare and the number of degrees of freedom, respectively.

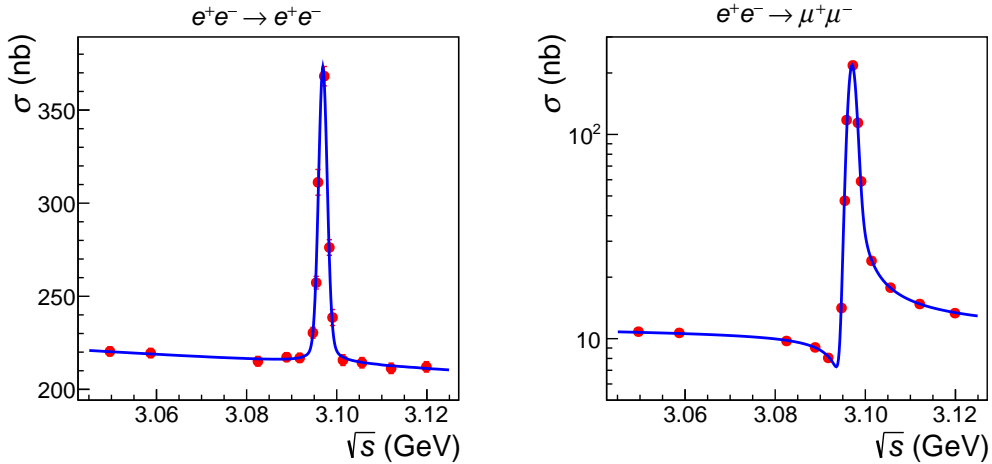


Fig. 3: Simultaneous fit to the measured, CM energy dependent cross sections of the processes $e^+e^- \rightarrow e^+e^-$ and $e^+e^- \rightarrow \mu^+\mu^-$. For clear display of the interference effect [denoted by σ_0^I in Eq. (3) and mainly illustrated by the small dip in front of the peak], the plot for the process $e^+e^- \rightarrow \mu^+\mu^-$ is drawn with a logarithmic vertical axis, while the plot for $e^+e^- \rightarrow e^+e^-$ is drawn with a linear vertical axis, because in this process the interference effect is less noticeable due to the existence of the scattering channel. In the plots, the red points with error bars and blue curves are from data and fitting, respectively.

Table 5: Comparison of the J/ψ decay widths obtained in this work with those from other experiments, the PDG and the BESIII work using the ISR return technique.

Collab.	Method	Year	Γ_{tot} (keV)	Γ_{ll} (keV)	Ref.
BaBar	ISR return	2004	94.7 ± 4.4	5.61 ± 0.21	[18]
CLEO	ISR return	2006	96.1 ± 3.2	5.71 ± 0.16	[19]
KEDR	ES	2010	94.1 ± 2.7	5.59 ± 0.12	[20]
BESIII	ISR return	2016	—	5.58 ± 0.09	[24]
KEDR	ES	2018	92.5 ± 2.0	5.55 ± 0.11	[21]
PDG	—	2020	92.9 ± 2.8	5.53 ± 0.10	[1]
This work	ES	2021	93.0 ± 2.1	5.56 ± 0.11	—

The fit result of $\Gamma_{ee}\Gamma_{ee}/\Gamma_{\text{tot}}$ and $\Gamma_{ee}\Gamma_{\mu\mu}/\Gamma_{\text{tot}}$ are (0.346 ± 0.009) and (0.335 ± 0.006) keV with the covariance and correlation coefficient between them as 0.000046 keV^2 and 0.83 , respectively. Taking into account the correlation term, we evaluate $\Gamma_{ee}/\Gamma_{\mu\mu}$ to be 1.031 ± 0.015 , which is consistent with the expectation of lepton universality within about 2σ . Besides, S_W is fitted to be $(0.916 \pm 0.018) \text{ MeV}$, which is consistent with the designed energy spread of the BEPCII collider, and F_{ee} and $F_{\mu\mu}$ are fitted to be 0.995 ± 0.009 and 1.015 ± 0.011 , respectively, which are compatible with the precision levels of the BABAYAGA-3.5 generator within uncertainties.

Assuming lepton universality, $\Gamma_{ee} = \Gamma_{\mu\mu}$, and referring to Γ_{ee} and $\Gamma_{\mu\mu}$ as Γ_{ll} , $\Gamma_{ee}\Gamma_{ee}/\Gamma_{\text{tot}}$ and $\Gamma_{ee}\Gamma_{\mu\mu}/\Gamma_{\text{tot}}$ are combined and referred to as $\Gamma_{ll}\Gamma_{ll}/\Gamma_{\text{tot}}$. The resultant $\Gamma_{ll}\Gamma_{ll}/\Gamma_{\text{tot}}$ is (0.332 ± 0.006) keV, which is smaller than the individual values of $\Gamma_{ee}\Gamma_{ee}/\Gamma_{\text{tot}}$ and $\Gamma_{ee}\Gamma_{\mu\mu}/\Gamma_{\text{tot}}$ because of the correlation between the latter two.

Combining the resultant $\Gamma_{ll}\Gamma_{ll}/\Gamma_{\text{tot}}$ with the branching ratio of the J/ψ leptonic decay measured by BESIII in 2013, $B(J/\psi \rightarrow l^+l^-) = \Gamma_{ll}/\Gamma_{\text{tot}} = (5.978 \pm 0.040) \%$ [30], Γ_{tot} and Γ_{ll} are determined to be (93.0 ± 2.1) and $(5.56 \pm 0.11) \text{ keV}$, respectively.

As mentioned previously, the impact of the systematic uncertainty (0.033 MeV) of the CM energies requires additional consideration. By increasing and decreasing the CM energies by 0.033 MeV , we repeat the entire simultaneous fit process twice, the relative changes of the results are less than 0.1% , and are neglected.

5.4. Result and comparison

The results obtained in this work are summarized as follows:

$$\begin{aligned}\Gamma_{ee}\Gamma_{ee}/\Gamma_{\text{tot}} &= (0.346 \pm 0.009) \text{ keV}, \\ \Gamma_{ee}\Gamma_{\mu\mu}/\Gamma_{\text{tot}} &= (0.335 \pm 0.006) \text{ keV}, \\ \Gamma_{ll}\Gamma_{ll}/\Gamma_{\text{tot}} &= (0.332 \pm 0.006) \text{ keV}, \\ \Gamma_{ee}/\Gamma_{\mu\mu} &= 1.031 \pm 0.015, \\ \Gamma_{\text{tot}} &= (93.0 \pm 2.1) \text{ keV}, \\ \Gamma_{ll} &= (5.56 \pm 0.11) \text{ keV}.\end{aligned}$$

The uncertainties quoted here are total uncertainties, which are obtained with all the statistical and systematic uncertainties of the input quantities taken into consideration.

The result of $\Gamma_{ee}/\Gamma_{\mu\mu}$ is consistent with and more precise than the result (1.002 ± 0.025) given by KEDR with the same method [20]. It is also in agreement with but less precise than the previous BESIII result (1.0017 ± 0.0037) obtained with a different approach [30]. Table 5 shows a comparison of the Γ_{tot} and Γ_{ll} obtained in this work with those from other works and the PDG. The results given by this work agree with all other results; they come up to a new precision level, together with previous results obtained with the ISR return technique at BESIII and ES method at KEDR.

6. Summary

Based on the data samples collected with the BESIII detector at fifteen CM energy points in the vicinity of the J/ψ resonance, the cross sections of the processes $e^+e^- \rightarrow e^+e^-$ and $e^+e^- \rightarrow \mu^+\mu^-$ are measured and summarized in Tables 2 and 3, respectively. By performing a simultaneous fit of the cross sections of the two processes as functions of the center-of-mass energy, $\Gamma_{ee}\Gamma_{ee}/\Gamma_{\text{tot}}$ and $\Gamma_{ee}\Gamma_{\mu\mu}/\Gamma_{\text{tot}}$ of the J/ψ resonance are determined to be (0.346 ± 0.009) and (0.335 ± 0.006) keV, respectively.

Using the obtained $\Gamma_{ee}\Gamma_{ee}/\Gamma_{\text{tot}}$ and $\Gamma_{ee}\Gamma_{\mu\mu}/\Gamma_{\text{tot}}$, the ratio of the J/ψ leptonic decay widths, $\Gamma_{ee}/\Gamma_{\mu\mu}$,

is evaluated to be 1.031 ± 0.015 , which agrees with the expectation of lepton universality within about two standard deviations. Under the assumption of lepton universality and combining with $B(J/\psi \rightarrow l^+l^-)$ measured by BESIII [30], the total and leptonic decay widths of the J/ψ resonance, Γ_{tot} and Γ_{ll} , are determined to be (93.0 ± 2.1) and (5.56 ± 0.11) keV, respectively. These results are consistent with the previous results and reach the world leading level.

7. Acknowledgments

The BESIII collaboration thanks the staff of BEPCII and the IHEP computing center for their strong support. This work is supported in part by National Key R&D Program of China under Contracts Nos. 2020YFA0406400, 2020YFA0406300; National Natural Science Foundation of China (NSFC) under Contracts Nos. 11275211, 11475090, 11335008, 11635010, 11735014, 11835012, 11935015, 11935016, 11935018, 11961141012, 12022510, 12025502, 12035009, 12035013, 12122509, 12192260, 12192261, 12192262, 12192263, 12192264, 12192265; the Chinese Academy of Sciences (CAS) Large-Scale Scientific Facility Program; Joint Large-Scale Scientific Facility Funds of the NSFC and CAS under Contract No. U1832207; 100 Talents Program of CAS; The Institute of Nuclear and Particle Physics (INPAC) and Shanghai Key Laboratory for Particle Physics and Cosmology; ERC under Contract No. 758462; European Union's Horizon 2020 research and innovation programme under Marie Skłodowska-Curie grant agreement under Contract No. 894790; German Research Foundation DFG under Contracts Nos. 443159800, Collaborative Research Center CRC 1044, FOR 2359, GRK 2149; Istituto Nazionale di Fisica Nucleare, Italy; Ministry of Development of Turkey under Contract No. DPT2006K-120470; National Science and Technology fund; National Science Research and Innovation Fund (NSRF) via the Program Management Unit for Human Resources & Institutional Development, Research and Innovation under Contract No. B16F640076; STFC (United Kingdom); Suranaree University of Technology (SUT), Thailand Science Research and Innovation (TSRI), and National Science Research and Innovation Fund (NSRF) under Contract No. 160355; The Royal Society, UK under Contracts Nos. DH140054, DH160214; The Swedish Research Council; U. S. Department of Energy under Contract No. DE-FG02-05ER41374

8. References

- [1] P.A. Zyla et al., Particle Data Group, Prog. Theor. Exp. Phys. 2020 (2020) 083C01.
- [2] N. Brambilla, et al., CERN Yellow Report, CERN-2005-005 (2005) 487; N. Brambilla, et al., Eur. Phys. J. C 71 (2011) 1534.
- [3] A.M. Badalian, I.V. Danilkin, Phys. Atom. Nucl. 72 (2009) 1206.
- [4] O. Lakhina, E.S. Swanson, Phys. Rev. D 74 (2006) 014012.
- [5] E. Eichten, K. Gottfried, T. Kinoshita, K.D. Lane and T.M. Yan, Phys. Rev. D 17 (1978) 3090; Phys. Rev. D 21 (1980) 313; Phys. Rev. D 21 (1980) 203.
- [6] J.L. Richardson, Phys. Lett. B 82 (1979) 272.
- [7] J.J. Dudek, R.G. Edwards, D.G. Richards, Phys. Rev. D 73 (2006) 074507.
- [8] A. Pich, NATO Sci. Ser. B 363 (1997) 173.
- [9] R. Van Royen, V.F. Weisskopf, Nuovo Cim. A 50 (1967) 617.
- [10] R.H. Bernstein, P.S. Cooper, Phys. Rept. 532 (2013) 27.
- [11] J.J. Aubert, et al., Phys. Rev. Lett. 33 (1974) 1404.
- [12] J.E. Augustin, et al., Phys. Rev. Lett. 33 (1974) 1406.
- [13] M. Boyarski et al., Phys. Rev. Lett. 34 (1975) 1357.
- [14] R. Baldini-Celio et al., Phys. Lett. B 58 (1975) 471.
- [15] B. Esposito et al., Lett. Nuovo Cim. 14 (1975) 73.
- [16] R. Brandelik et al., Z. Phys. C 1 (1979) 233.
- [17] J.Z. Bai et al., BES Collaboration, Phys. Lett. B 355 (1995) 374.
- [18] B. Aubert, et al., BaBar Collaboration, Phys. Rev. D 69 (2004) 011103.
- [19] G.S. Adams, et al., CLEO Collaboration, Phys. Rev. D 73 (2006) 051103.
- [20] V.V. Anashin, et al., KEDR Collaboration, Phys. Lett. B 685 (2010) 134.
- [21] V.V. Anashin, et al., KEDR Collaboration, J. High Energ. Phys. 05 (2018) 119 [Addendum: J. High Energ. Phys. 07 (2020) 112].
- [22] C. Zhang, Sci. China Phys. Mech. Astron. 53 (2010) 2084.
- [23] M. Ablikim, et al., BESIII Collaboration, Nucl. Instrum. Methods A 614 (2010) 345.
- [24] M. Ablikim, et al., BESIII Collaboration, Phys. Lett. B 761 (2016) 98.
- [25] R.P. Feynman, Photon-Hadron Interactions, Boulder, Colorado: Westview Press, 1998.
- [26] V.V. Anashin, et al., KEDR Collaboration, Phys. Lett. B 711 (2012) 280.
- [27] X.Y. Zhou, Y.D. Wang, L.G. Xia, Chin. Phys. C 41 (2017) 083001.
- [28] E.A. Kuraev, V.S. Fadin, Sov. J. Nucl. Phys., 41 (1985) 466.
- [29] F.Z. Chen, P. Wang, J.M. Wu, et al., HEP & NP 14 (7) (1990) 585 (in Chinese) and BIHEP-EP-90-01 (preprint in English).
- [30] M. Ablikim, et al., BESIII Collaboration, Phys. Rev. D 88 (2013) 032007.
- [31] E.V. Abakumova, et al., Nucl. Instrum. Methods A 659 (2011) 21.
- [32] M. Ablikim, et al., BESIII Collaboration, Phys. Rev. D 90 (2014) 012001.
- [33] M. Ablikim, et al., BESIII Collaboration, Chin. Phys. C 41 (2017) 063001.
- [34] C.M. Carloni Calame, et al., Nucl. Phys. B 584 (2000) 459; C.M. Carloni Calame, Phys. Lett. B 520 (2001) 16; C.M. Carloni Calame, et al., Nucl. Phys. B (Proc. Suppl.) 131 (2004) 48.
- [35] R.G. Ping, Chin. Phys. C 38 (2014) 083001, R.G. Ping, et al., Chin. Phys. C 40 (2016) 113002.
- [36] J.J. Sakurai, D. Schildknecht, Phys. Lett. B 40 (1972) 121.
- [37] S. Agostinelli, et al., GEANT4 Collaboration, Nucl. Instrum. Meth. A 506 (2003) 250.
- [38] G. Barrand, et al., Comput. Phys. Commun. 140 (2001) 45.
- [39] X.Y. Zhou, S.X. Du, G. Li, C.P. Shen, Comput. Phys. Commun. 258 (2021) 107540.
- [40] N. Berger, et al., Chin. Phys. C 34 (2010) 1779.